*J Mater Sci* (2022) 57:2012–2020

Energy materials

# α-$Fe_2O_3$/alkalinized $C_3N_4$ heterostructure as efficient electrocatalyst for oxygen reduction reaction

Feng Chen[1,*], Congcong Yao[1], Junchao Qian[1,*], Jiajia Fan[1], Xingwang Chen[1], Wenjie Wu[2], Li Xu[3], Qianqian Liu[4], and Wanfei Li[4,*]

[1] *Jiangsu Key Laboratory for Environment Functional Materials, Suzhou University of Science and Technology, Suzhou, Jiangsu Province 215009, China*

[2] *Engineering Research Center for Nanophotonics and Advanced Instrument, Ministry of Education, School of Physics and Materials Science, East China Normal University, Shanghai 200062, China*

[3] *School of Chemistry and Chemical Engineering, Institute for Energy Research, Jiangsu University, Zhenjiang, Jiangsu Province 212013, China*

[4] *Suzhou Key Laboratory for Nanophotonic and Nanoelectronic Materials and Its Devices, School of Materials Science and Engineering, Suzhou University of Science and Technology, Jiangsu Province 215009, China*

**Received:** 3 September 2021
**Accepted:** 25 October 2021
**Published online:**
3 January 2022



## ABSTRACT

A nanocomposite of α-$Fe_2O_3$/alkalinized $C_3N_4$ (α-$Fe_2O_3$/A-$C_3N_4$) electrocatalyst for oxygen reduction reaction (ORR) was synthesized by a simple in situ electrostatic adsorption of A-$C_3N_4$ and iron-based ionic liquid [Omim]$FeCl_4$ complexation reaction using sonication treatment followed by pyrolysis process. The as-prepared α-$Fe_2O_3$/A-$C_3N_4$ nanocomposite can act as a superior electrocatalyst for ORR in terms of excellent ORR activity with onset potential of 0.82 V vs. reversible hydrogen electrodes (RHE), current density of 5.2 mA $cm^{-2}$ and outstanding methanol resistance. This cost-effective starting materials and simple preparation method paves the way to large-scale fabrication of low-cost and highly active noble metal-free electrocatalyst and promotes their practical applications in electrochemical power conversion and storage system.

Handling Editor: Joshua Tong.

Feng Chen and Congcong Yao have contributed to this work equally.

Address correspondence to E-mail: chenfeng@mail.usts.edu.cn; qianjunchao1983@mail.usts.edu.cn; wfli2018@mail.usts.edu.cn



https://doi.org/10.1007/s10853-021-06666-8

## GRAPHICAL ABSTRACT

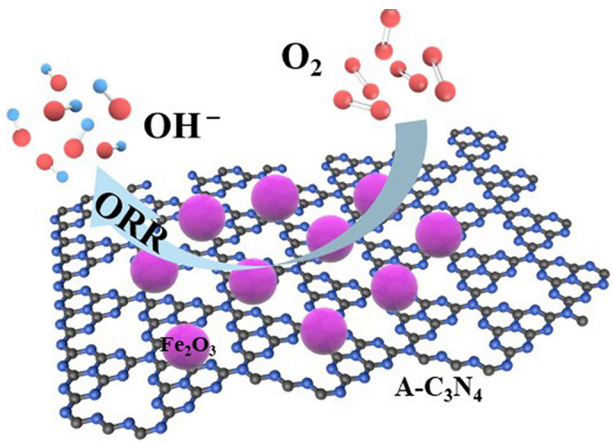


## Introduction

The demand for clean energy is growing at a high speed in recent years owning to limited fossil fuel and environmental pollution [1]. Seeking for a high-efficiency, low cost and environmental friendly energy conversion technology is the most critical and urgent challenge [2, 3]. Oxygen reduction reaction (ORR) is the key factor in both fuel cells and metal-air batteries. However, the ORR progress exhibits the slow kinetics and high over-potential, which controls the efficiency of the energy devices [4]. To date, the outstanding catalysts for ORR are still based on the precious metal platinum (Pt) and its alloys. For example, Du et al. found that PtCo@NC deriving from Co-based zeolitic imidazolate framework material (ZIF-67) can highly catalyze ORR in both acid and alkaline electrolyte and exhibited highly stability after 10000 cycles [5]. It has also been reported recently that Pt skin coated Ag-Pt nanoparticles shows ultrahigh catalytic activity for ORR [6]. However, the high costs and scarcity of noble platinum as well as its easily suffering poisoning effects are big obstacles, which hinders its widely application [7]. Therefore, developing noble metal-free catalysts with low-cost and comparable high activity is still full of challenge.

Meanwhile, the earth-abundant non-noble metal oxides (MO), such as $Co_3O_4$ [8], $Mn_3O_4$ [9] etc. have been extensively investigated on electrocatalysis. Among the as-reported metal oxides ORR catalysts, $\alpha$-$Fe_2O_3$ has been regarded as an ideal alternative to replace the use of Pt because of its high-efficiency, low-cost and eco-friendly characteristics [10]. However, the intrinsic properties including poor electrical conductivity, less active site density and the dissolution or agglomeration during electrochemical processes of these metal oxides-based catalysts limited their practical application [11–13]. Two-dimensional (2D) carbon nitride ($C_3N_4$) can be used as substrate to afford metal oxide nanoparticles homogeneously dispersing, thus being used for promising electrocatalyst composites [14]. In addition, the high nitrogen doping amount of $C_3N_4$ makes it as a promising electrode material for energy storage [15]. However, the literature about ORR performance of $C_3N_4$ was found to be very sparse due to its low conductivity [16]. To overcome this shortcoming, many articles reported that introducing conductive carbon materials or catalysts loaded on other conductive substrate can enhance their electrocatalytic activity [17].

Herein, $\alpha$-$Fe_2O_3$ nanoparticles with uniform-size were successfully loaded on 2D A-$C_3N_4$ nanosheets through sonication and pyrolysis treatment to afford a novel $\alpha$-$Fe_2O_3$/A-$C_3N_4$ nanocomposites. Amounts of hydroxyl on the surface of A-$C_3N_4$ after alkalinization facilitates the uniform electrostatic adsorption of iron ion in ionic liquid [Omim]$FeCl_4$ via complexation reaction, which contributes to uniform

dispersion of α-$Fe_2O_3$ nanoparticles on the A-$C_3N_4$ nanosheets. The as-prepared α-$Fe_2O_3$/A-$C_3N_4$ nanocomposite exhibited excellent ORR activity. Furthermore, acetylene black (AB) as the conductive carbon material additive was introduced to improve the conductivity. Then, the ORR activity of α-$Fe_2O_3$/A-$C_3N_4$ loading onto AB was investigated through CV, LSV and *i-t* tests in 0.1 M $N_2/O_2$ atmosphere saturated KOH aqueous. The α-$Fe_2O_3$/A-$C_3N_4$ composites loading onto AB showed excellent ORR activity with onset potential of 0.82 V vs. RHE, current density of 5.2 mA $cm^{-2}$ and outstanding methanol resistance.

## Experimental section

### Materials

Anhydrous ferric chloride hexahydrate and potassium hydroxide were directly used without any further modification. 1-Butyl-3-methylimidazolium chloride ([Omim]Cl) was purchased from Shanghai Cheng Jie Chemical Co. LTD.

### Preparation of [Omim]$FeCl_4$

Equimolar amounts of [Omim]Cl and $FeCl_3 \cdot 6H_2O$ were added into a 100 mL round bottom flask, and then refluxed at 100 °C for 6 h. The product was subsequently filtered and dried in an oven to get a homogeneous brown liquid. The final dark brown liquid was remarked as [Omim]$FeCl_4$.

### Preparation of A-$C_3N_4$

$C_3N_4$ was originated from directly annealing urea in a tube furnace with a certain flow of $N_2$. Specifically, 3 g urea powder was set into alumina crucible with cover and calcined at 350 °C for 2 h. The temperature was subsequently raised to 600 °C and retained for another 2 h. After cooling down to ambient condition, the light-yellow $C_3N_4$ was collected. Secondly, 0.2 g previously obtained $C_3N_4$ powder was leached in a certain concentration of KOH aqueous for 12 h under vigorous stirring. The alkalinized $C_3N_4$ product was isolated by filtering and repeatedly washed to neutral with distilled water and absolute ethanol separately, dried and sealed for use. And the alkalinized $C_3N_4$ was denoted as A-$C_3N_4$.

### Preparation of the hematite α-$Fe_2O_3$/A-$C_3N_4$

Firstly, a certain amount of [Omim]$FeCl_4$ (fixed as 0.2 g, 0.5 g, 0.8 g) was added into 1.5 mL ultrapure water and then quantitative A-$C_3N_4$, and the formed homogeneous solution was ultrasonicated for 6 h to make the iron-based ion liquid absorbed on the surface of A-$C_3N_4$. Finally, put the mixture of iron-based ion liquid and A-$C_3N_4$ into a muffle furnace with a heating rate of 2 °C/min to reach T °C (T was adjusted according to 250, 300, 350 °C) and maintained for 2 h. When cooled down sufficiently, the black product was collected after washed and dried, the final product was denoted as X α-$Fe_2O_3$/A-$C_3N_4$-T.

### ORR performance

All the ORR measurements were carried out using CHI 760E workstation in a typical three-electrode system. Specifically, Ag/AgCl electrode with internal solution of 3 M KCl was used reference electrode. Platinum wire was used as counter electrode. Meanwhile, the as-prepared catalysts α-$Fe_2O_3$/A-$C_3N_4$ modified glass carbon electrode (GC) was used as indicator electrode. The indicator electrode was prepared as follows: dispersing 4 mg catalyst into 1 mL mixture of water, isopropanol and Nafion (10 wt%) solution with volume ratio of 150/50/3 to form a 4 mg $mL^{-1}$ homogeneous suspension. Then, a 10 μL suspension was carefully dropped onto GC electrode with diameter of 3 mm, and the loading amount was calculated about 40 μg. The indicator electrode was dried naturally under ambient conditions for further tests. Before being modified, the GC electrode was polished using alumina slurry to remove the inactive residual, followed by ultrasound in ethanol for several seconds. The CV and LSV tests were conducted in 0.1 M KOH solution with potential range from 0.17 to 1.17 V vs. RHE.

## Results and discussion

### XRD spectra analysis

Structural characteristics and phase compositions of all as-prepared α-$Fe_2O_3$/A-$C_3N_4$ composites were analyzed by X-ray diffraction (XRD, XRD-6100 Lab, shimadzu, Japan). As shown by Fig. 1A, the typical

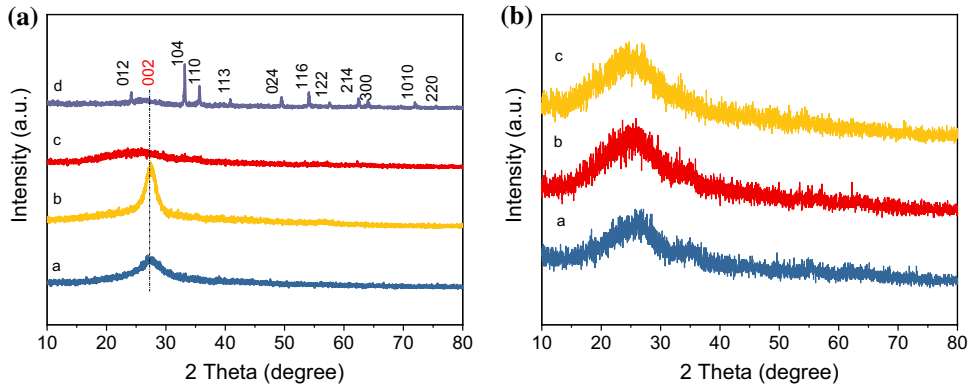


**Figure 1** **A** XRD patterns of A-$C_3N_4$ (a) and 0.5 α-$Fe_2O_3$/A-$C_3N_4$-T with different temperature (b: $T$ = 250; c: $T$ = 300; d: $T$ = 350); **B** XRD patterns of $X$ α-$Fe_2O_3$/A-$C_3N_4$-300 with different ionic liquid content (a: $X$ = 0.2; b: $X$ = 0.5; c: $X$ = 0.8).

peak at ~ 27.3 ° was the diffraction peak of A-$C_3N_4$, which was indexed to (002) crystal surface [18]. The other detective peaks appeared at 24.2°, 33.1°, 35.6°, 40.8°, 49.5°, 54.0°, 57.6°, 62.5°, 64.0°, 72.1°, and 75.6° were completely consistent with JCPDS NO. 33-0664 of hematite α-$Fe_2O_3$ [19]. Meanwhile, the typical peak of A-$C_3N_4$ had a slight shift due to the enlarged interlayer spacing. Furthermore, the XRD spectra of the products annealed at 300 °C with different ionic liquid content were shown in Fig. 1B. It also showed ambiguous characteristic peaks of hematite α-$Fe_2O_3$ due to low calcination temperature.

## XPS spectra analysis

X-ray photon spectrum (XPS) has been widely used to identify the element species and valence states of as-prepared α-$Fe_2O_3$/A-$C_3N_4$ composites due to its high accuracy. The 0.5 α-$Fe_2O_3$/A-$C_3N_4$-300 catalyst was characterized by XPS analysis (ESCALAB MK II, VG Scientific, England) as shown in Fig. 2. Four significant peaks of C, N, O and Fe were detected in Fig. 2A. Furthermore, its high-resolution spectra are shown in Fig. 2B-E. In detail, XPS of Fe species showed two strong peaks at nearly 725.0 eV and 711.3 eV (Fig. 2B), which were assigned to Fe $2p_{1/2}$ and Fe $2p_{3/2}$, demonstrating the valence state of iron was + 3 [20]. In addition, the O 1 s high resolution spectrum in Fig. 2C showed dominant oxide peaks at around 531.4 eV, consistent with the $O^{2-}$ state. The C 1 s high resolution spectrum in Fig. 2D showed that C–C (284.7 eV), C-N (286.2 eV) and C-O (287.9 eV) bonds existed in the A-$C_3N_4$ of 0.5 α-$Fe_2O_3$/A-$C_3N_4$-300. Similarly, N 1 s showed two typical peaks at 398.6 and 400.9 eV (Fig. 2E), which were consistent with pyridinic and graphitic-like N, respectively [21]. Both the two high resolution of N 1 s and C 1 s characterized the presence of carbon nitride [22]. Therefore, XPS characterization results absolutely demonstrated that the α-$Fe_2O_3$/A-$C_3N_4$ has been successfully prepared through ultrasound-pyrolysis fabrication.

Fourier transform infrared spectra (FT-IR, Nicolet Nexus 470, Thermo Nicolet Corporation, America) have been widely used to identify the functional groups of α-$Fe_2O_3$/A-$C_3N_4$. Figure 3 shows the FT-IR spectra of pure A-$C_3N_4$ and α-$Fe_2O_3$/A-$C_3N_4$. In the case of pure A-$C_3N_4$, the strong bands in the 1200–1600 $cm^{-1}$ region are found in the spectra, which correspond to the typical stretching vibration modes of C = N and C-N heterocycles [23]. Additionally, the characteristic breathing mode of triazine units at 810 $cm^{-1}$ are observed. In the FT-IR spectra of α-$Fe_2O_3$/A-$C_3N_4$, it can also be clearly seen that the main characteristic peaks of A-$C_3N_4$ appear in all α-$Fe_2O_3$/A-$C_3N_4$. It strongly indicates the α-$Fe_2O_3$/A-$C_3N_4$ has been successful synthesized, which is consistent with XPS analysis.

## Surface and interior morphology analysis

The surface morphology structure of alkalized graphitic carbon nitride (A-$C_3N_4$) and 0.5 α-$Fe_2O_3$/A-$C_3N_4$-300 composites were observed by Transmission electron microscope (TEM, JEOL-JEM-2010, Japan). As shown in Fig. 4a and b, A-C3N4 was composed of nanosheets with rugged folds. After introducing Fe-based ionic liquid, the original A-$C_3N_4$ nanosheets were stacked into α-$Fe_2O_3$/A-$C_3N_4$ nanocomposites (Fig. 4c and d). The α-$Fe_2O_3$ nanoparticles are uniformly distributed on A-$C_3N_4$ nanosheets.

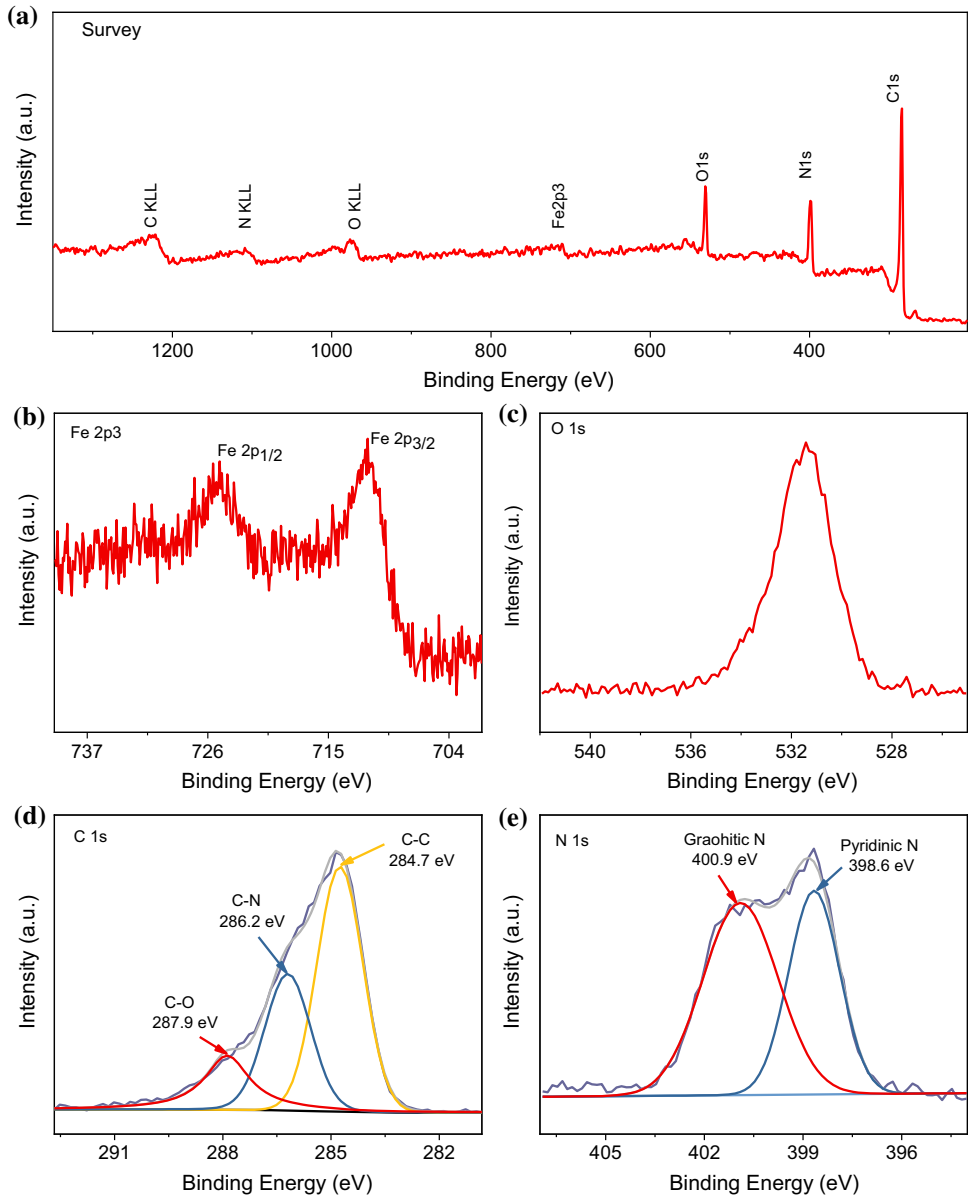


**Figure 2** **A** Survey XPS spectra of A-$C_3N_4$ (a) and 0.5 α-$Fe_2O_3$/A-$C_3N_4$-300 (b); **B**–**E** high resolution of Fe, O, C and N elements.

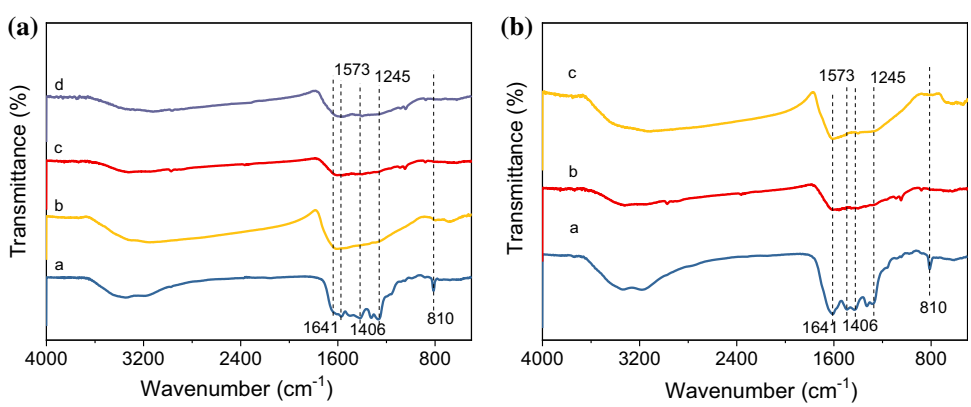


**Figure 3** **A** FT-IR spectra of A-$C_3N_4$ (a) and 0.5 α-$Fe_2O_3$/A-$C_3N_4$-T with different temperature (b: $T$ = 250; c: $T$ = 300; d: $T$ = 350); **B** FT-IR spectra of $X$ α-$Fe_2O_3$/A-$C_3N_4$-300 with different ionic liquid content (a: $X$ = 0.2; b: $X$ = 0.5; c: $X$ = 0.8).

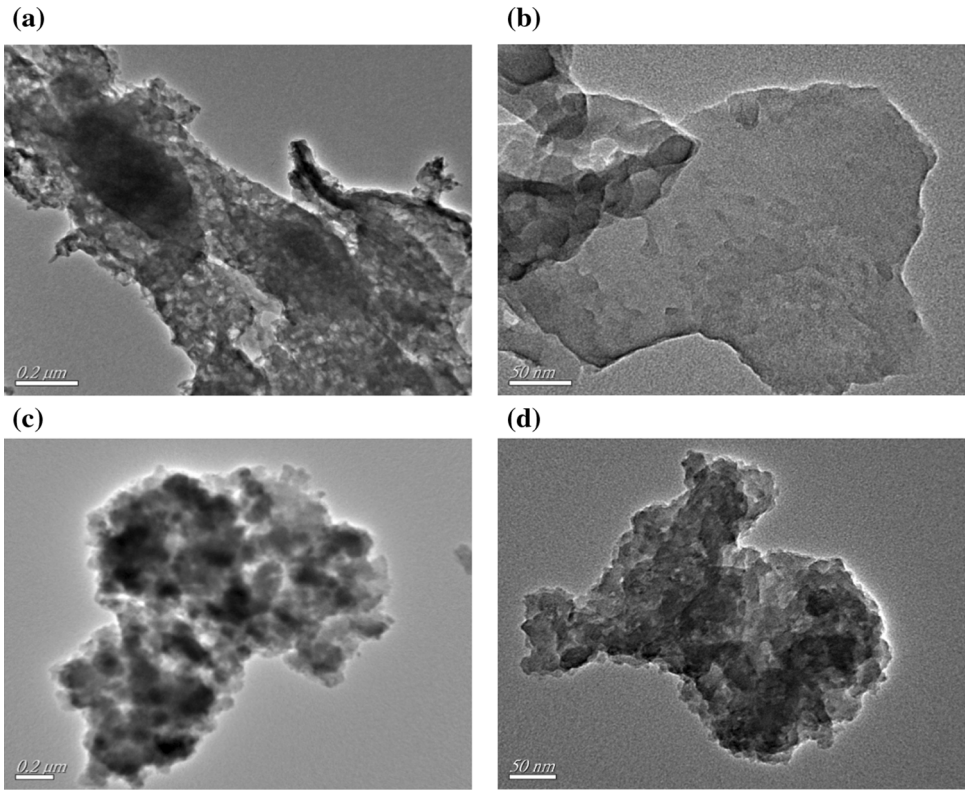


**Figure 4** TEM pictures of A-$C_3N_4$ (**a**, **b**) and 0.5 α-$Fe_2O_3$/ A-$C_3N_4$-300 (**c**, **d**).

## ORR performance evaluation

High nitrogen content and porous structure of catalyst for ORR was confirmed to be very significant. The LSV was adopted to assess the ORR performance of α-$Fe_2O_3$/A-$C_3N_4$ nanocomposite. To explore whether the nanocomposite of α-$Fe_2O_3$/A-$C_3N_4$ can catalyze oxygen reduction or not, the LSV was conducted under $O_2$ saturated alkaline electrode. As shown in Fig. 5a, the α-$Fe_2O_3$/A-$C_3N_4$ exhibited a much more positive onset potential than A-$C_3N_4$. That is to say, the α-$Fe_2O_3$/A-$C_3N_4$ exhibited ORR activity due to the unique hybrid structure of α-$Fe_2O_3$ and A-$C_3N_4$. Meanwhile, α-$Fe_2O_3$/A-$C_3N_4$ in 300 °C of calcination temperature displays obviously higher activity than other α-$Fe_2O_3$/A-$C_3N_4$. With increase of the calcination temperature, the A-$C_3N_4$ can be decomposed, resulting in a significant decrease of catalytic activity. The LSV of α-$Fe_2O_3$/A-$C_3N_4$ with different contents of ionic liquid is shown in Fig. 5b. The data showed that the α-$Fe_2O_3$/A-$C_3N_4$ with 0.5 g of ionic liquid displayed obviously higher activity than other α-$Fe_2O_3$/A-$C_3N_4$. Thus, the α-$Fe_2O_3$/A-$C_3N_4$ obtained by calcined with 0.5 g of ionic liquid at 300 °C exhibited the best ORR activity. Moreover, the ORR performance evaluation parameters of α-$Fe_2O_3$/A-$C_3N_4$ catalyst, such as onset potential and current

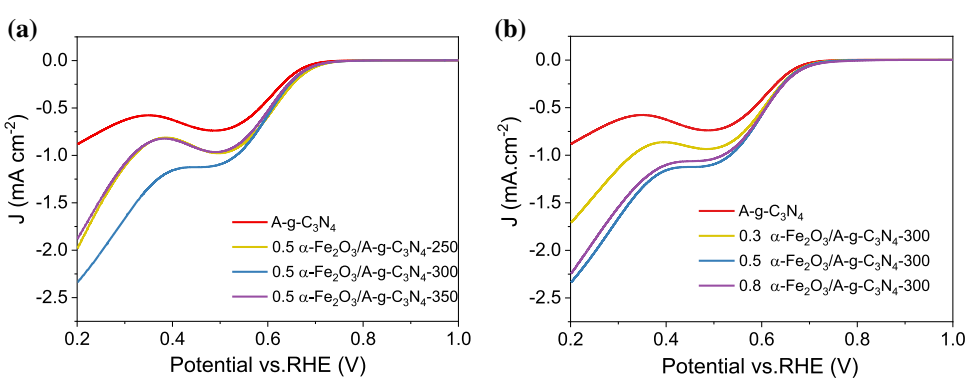


**Figure 5** **a** LSV results of α-$Fe_2O_3$/A-$C_3N_4$ composites by calcined in different temperature (250, 300, and 350 °C); **b** LSV results of α-$Fe_2O_3$/A-$C_3N_4$ composites by calcined with different contents of ionic liquid (0.2, 0.5, and 0.8 g).

**Table 1** Comparison of α-$Fe_2O_3$/A-$C_3N_4$ with similar catalysts that have been reported for ORR activity

| Catalysts | Onset potential | Current density (mA $cm^{-2}$) | Testing Conditions | Ref. |
|---|---|---|---|---|
| α-$Fe_2O_3$/A-$C_3N_4$ | 0.82 V vs. RHE | 5.2 | 0.1 M KOH | This work |
| α-$Fe_2O_3$@N–C | 0.80 V vs. RHE | 5.67 | 0.1 M KOH | [19] |
| α-$Fe_2O_3$@C | −0.241 V vs. Hg/HgO | – | 0.5 M KOH | [24] |
| α-$Fe_2O_3$/CNTs | − 0.15 V vs. Ag/AgCl | − 3.89 | 0.1 M KOH | [25] |
| α-$Fe_2O_3$/N-CNTs | − 0.16 V vs. Ag/AgCl | − 3.1 | 0.1 M KOH | [26] |
| α-$Fe_2O_3$/GO | − 0.1 V vs. Hg/HgO | − 3.6 | 0.1 M KOH | [27] |

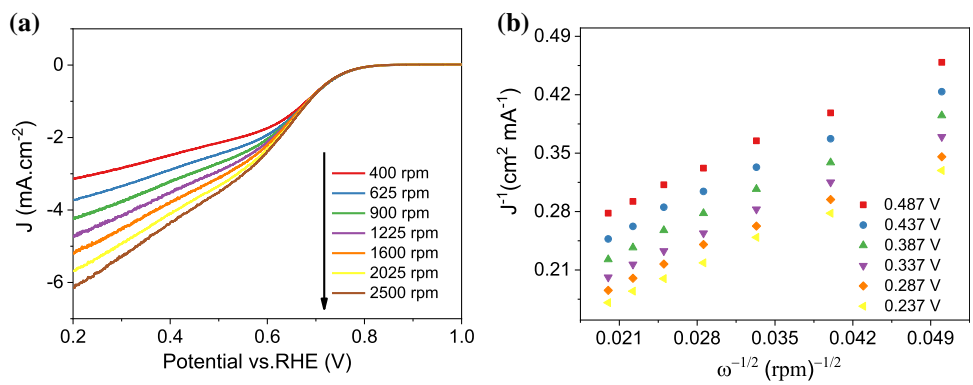


**Figure 6** **a** LSV with $O_2$ at a scan rate of 10 mV.s$^{-1}$ of 0.5 α-$Fe_2O_3$/A-$C_3N_4$-300 under 0.1 M KOH aqueous; **b** The corresponding Koutecky–Levich plot of $J^{-1}$ versus $\omega^{-1/2}$ from 0.487 to 0.237 V vs. RHE.

density, have been compared with similar catalysts that have been reported and are listed in Table 1.

This series of catalysts possessed limited ORR activity due to their semiconductor property of α-$Fe_2O_3$/A-$C_3N_4$. The acetylene black was introduced to alleviate the problem. And the LSV was conducted to assess the ORR activity of 0.5 α-$Fe_2O_3$/A-$C_3N_4$-300 in the presence of AB (Fig. 6). Figure 6a shows that the measured current density (J) is enhanced with the increase of rotation rate (ω), with well-defined diffusion-limiting current plateau. Koutecky–Levich plots reveal well linearity between $J^{-1}$ and $\omega^{-1/2}$ from 0.487 to 0.237 V vs. RHE (Fig. 6a).

All electrochemical performance indicated that introducing conductive carbon of AB can improve its ORR activity. In addition, to verify the reaction process during oxygen reduction, Rotating ring disk electrode (RRDE, RRDE-3A, Hailan Jiasheng Technology Co., Ltd., Beijing) test was recorded in Fig. 7a, and the corresponding $H_2O_2$ yield, and electron transfer number $n$ were calculated about 20% and 3.7 respectively. And the calculation is as follows:

$$HO_2^-(\%) = 200 * \frac{I_{ring}/N}{I_{disk} + I_{ring}/N} \ldots n = 4 * \frac{I_{disk}}{I_{disk} + I_{ring}/N}$$

This result indicated that the ORR was dominated by quasi-four-electron process. Meanwhile, its stability of methanol tolerance and acceleration degradation test was conducted under $O_2$ saturated electrolyte. As can be seen from Fig. 7c, the *i-t* curve was almost kept unchanged after injecting a certain methanol. When applying potential to *i-t* test, the retention current can be maintained above 86% after 10000 s. The results illustrate that the catalyst shows good catalytic stability.

## Conclusion

In summary, we synthesized the α-$Fe_2O_3$/A-$C_3N_4$ nanocomposite through sonication and pyrolysis with iron-based ionic liquid [Omim]$FeCl_4$. In-situ adsorbed iron elements of [Omim]$FeCl_4$ on the surface of alkalinized A-$C_3N_4$ via electrostatic interaction can result in uniform dispersion of α-$Fe_2O_3$ on the surface of A-$C_3N_4$. Efficient combination of α-$Fe_2O_3$ nanoparticles and A-$C_3N_4$ nanosheets can

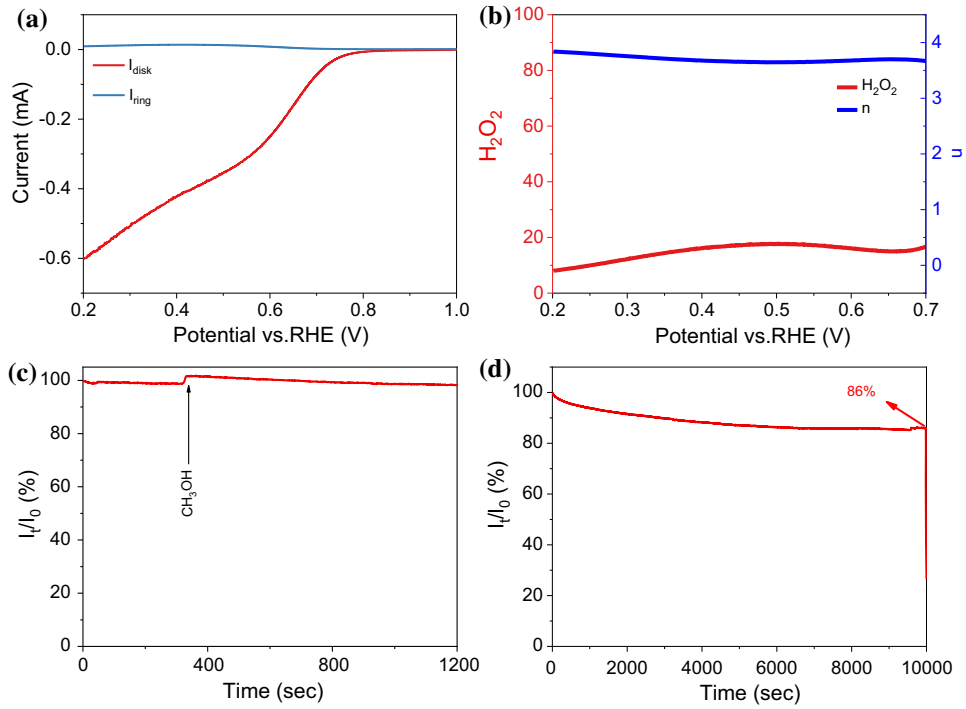


**Figure 7** **a** RRDE test of 0.5 α-$Fe_2O_3$/A-$C_3N_4$-300 at a scan rate of 10 mV $s^{-1}$ with additional ring potential of 0.749 V vs. RHE. **b** $H_2O_2$ yield (20%) and electron transfer number *n* (3.7) calculated according to (**a**). Stability of methanol tolerance (**c**) and acceleration degradation test (**d**) in 0.1 M KOH electrolyte.

enhance electrocatalytic ORR properties. Introducing AB can improve its intrinsic conductivity facilitating the electrocatalytic performance-enhancing. These electrochemical investigations evidently indicated the positive effects of α-$Fe_2O_3$/A-$C_3N_4$ catalyst on the catalytic ORR activity via the four-electron ORR process. α-$Fe_2O_3$/A-$C_3N_4$ nanocomposite, in which both α-$Fe_2O_3$ and A-$C_3N_4$ are easily prepared from low-cost raw materials, could be a potential candidate to replace noble metal platinum in energy conversion and storage system.

## Acknowledgements

This work was supported by Natural Science Foundation of China (21773291,22002102); The Natural Science Foundation of Jiangsu Province (Grants No. BK20180103, BK20180971); Jiangsu Collaborative Innovation Center of Technology and Material for Water Treatment (XTCXSZ2019-1); Innovation Training Project of Jiangsu Province (202010332071Y); Inner Mongolia Autonomous Region Key Laboratory of Nanocarbon Materials (No. MDK2019008).

## Declarations

**Conflict of interest** The authors declare that there is no conflict of interest.

## References

[1] Amiri M, Konda SK, Chen A (2017) Facile synthesis of a carbon nitride/reduced graphene oxide/nickel hydroxide nanocomposite for oxygen reduction in alkaline media. ChemElectroChem 4(5):997–1001

[2] Xiao Z, Hou F, Li Y, Zhang R, Shen G, Wang L, Zhang X, Wang Q, Li G (2019) Confinement of $Fe_2O_3$ nanoparticles in the shell of N-doped carbon hollow microsphere for efficient oxygen reduction reaction. Chem Eng Sci 207:235–246

[3] Chuong ND, Thanh TD, Kim NH, Lee JH (2018) Hierarchical heterostructures of ultrasmall $Fe_2O_3$-encapsulated $MoS_2$/N-Graphene as an effective catalyst for oxygen reduction reaction. ACS Appl Mater Interfaces 10(29):24523–24532

[4] Wan H, Lv MH, Liu XH, Chen G, Zhang N, Cao YJ, Wang HD, Ma RZ, Qiu GZ (2019) Activating hematite nanoplates via partial reduction for electrocatalytic oxygen reduction reaction. ACS Sustain Chem Eng 7:11841–11849

[5] Du N, Wang C, Long R, Xiong Y (2017) N-doped carbon-stabilized PtCo nanoparticles derived from Pt@ZIF-67: highly active and durable catalysts for oxygen reduction reaction. Nano Res 10(9):3228–3237

[6] Fu T, Huang J, Lai S, Zhang S, Fang J, Zhao J (2017) Pt skin coated hollow Ag-Pt bimetallic nanoparticles with high catalytic activity for oxygen reduction reaction. J Power Sources 365:17–25

[7] Barbosa ECM, Parreira LS, de Freitas IC, Aveiro LR, de Oliveira DC, dos Santos MC, Camargo PHC (2019) Pt-Decorated $TiO_2$ materials supported on carbon: increasing activities and stabilities toward the ORR by tuning the Pt loading. ACS Appl Energy Mater 2(8):5759–5768

[8] Wang Y, Yin X, Shen H, Jiang H, Yu J, Zhang Y, Li D, Li W, Li J (2018) $Co_3O_4$@g-$C_3N_4$ supported on N-doped graphene as effective electrocatalyst for oxygen reduction reaction. Int J Hydrogen Energy 43(45):20687–20695

[9] Bikkarolla SK, Yu F, Zhou W, Joseph P, Cumpson P, Papakonstantinou P (2014) A three-dimensional $Mn_3O_4$ network supported on a nitrogenated graphene electrocatalyst for efficient oxygen reduction reaction in alkaline media. J Mater Chem A 2(35):14493–14501

[10] Ye CC, Liu JZ, Zhang QH, Jin XJ, Zhao Y, Pan ZH, Chen GX, Qiu YC, Ye DQ, Gu L, Waterhouse GIN, Yang SH (2021) Activating metal oxides nanocatalysts for electrocatalytic water oxidation by quenching-induced near-surface metal atom functionality. J Am Chem Soc 143(35):14169–14177

[11] Zha R, Shi T, He L, Sun X, Jia Y, Zhang M (2020) Engineering the surface active sites of actiniae-like hierarchical $Fe_3O_4/Co_3O_4$ nanoheterojunction for efficient oxygen reduction reaction. Dyes Pigments 180:108439.

[12] Dhavale VM, Singh SK, Nadeema A, Gaikwada SS, Kurungot S (2015) Nanocrystalline Fe-$Fe_2O_3$ particle-deposited N-doped graphene as an activity-modulated Pt-free electrocatalyst for oxygen reduction reaction. Nanoscale 7:20117–20125

[13] Wang MW, Su C, Saunders M, Liang J, Shao ZP, Wang SB, Liu J (2017) Yolk-Shell-Structured Cu/Fe@$\gamma$-$Fe_2O_3$ Nanoparticles loaded graphitic porous carbon for the oxygen reduction reaction. Part Part Syst Charact 34:1700158

[14] Qiu Y, Xin L, Jia F, Xie J, Li W (2016) Three-dimensional phosphorus-doped graphitic-$C_3N_4$ self-assembly with $NH_2$-functionalized carbon composite materials for enhanced oxygen reduction reaction. Langmuir 32(48):12569–12578

[15] Li J, Zhang Y, Zhang X, Han J, Wang Y, Gu L, Zhang Z, Wang X, Jian J, Xu P, Song B (2015) Direct transformation from Graphitic $C_3N_4$ to nitrogen-doped graphene: an efficient metal-free electrocatalyst for oxygen reduction reaction. ACS Appl Mater Interfaces 7(35):19626–19634

[16] Qu L, Zhang Z, Zhang H, Zhang H, Dong S (2018) Transformation from graphitic $C_3N_4$ to nitrogen-boron-carbon ternary nanosheets as efficient metal-free bifunctional electrocatalyst for oxygen reduction reaction and hydrogen evolution reaction. Appl Surf Sci 448:618–627

[17] Zhang F, Miao J, Liu W, Xu D, Li X (2019) Heteroatom embedded graphene-like structure anchored on porous biochar as efficient metal-free catalyst for ORR. Int J Hydrogen Energy 44(59):30986–30998

[18] Wen J, Xie J, Chen X, Li X (2017) A review on g-$C_3N_4$-based photocatalysts. Appl Surf Sci 391:72–123

[19] Fu Y, Wang J, Yu H-Y, Li X, Wang H, Tian J-H, Yang R (2017) Enhanced electrocatalytic performances of $\alpha$-$Fe_2O_3$ pseudo-nanocubes for oxygen reduction reaction in alkaline solution with conductive coating. Int J Hydrogen Energy 42(32):20711–20719

[20] Chong R, Wang B, Su C, Li D, Mao L, Chang Z, Zhang L (2017) Dual-functional CoAl layered double hydroxide decorated $\alpha$-$Fe_2O_3$ as an efficient and stable photoanode for photoelectrochemical water oxidation in neutral electrolyte. J Mater Chem A 5(18):8583–8590

[21] Lu Z, Song W, Ouyang C, Wang H, Zeng D, Xie C (2017) Enhanced visible-light photocatalytic performance of highly-dispersed Pt/g-$C_3N_4$ nanocomposites by one-step solvothermal treatment. RSC Adv 7(53):33552–33557

[22] Wang X, Cheng J, Yu H, Yu J (2017) A facile hydrothermal synthesis of carbon dots modified g-$C_3N_4$ for enhanced photocatalytic $H_2$-evolution performance. Dalton Trans 46(19):6417–6424

[23] Yu H, Shi R, Zhao Y, Bian T, Zhao Y, Zhou C, Waterhouse GIN, Wu L-Z, Tung C-H, Zhang T (2017) Alkali-assisted synthesis of nitrogen deficient graphitic carbon nitride with tunable band structures for efficient visible-light-driven hydrogen evolution. Adv Mater 29(16):1605148

[24] Jang B, Bong S, Woo S, Park S-K, Ha J, Choi E et al (2014) Facile synthesis of one-dimensional iron-oxide/carbon hybrid nanostructures as electrocatalysts for oxygen reduction reaction in alkaline media. J Nanosci Nanotechnol 14(11):8852–8857

[25] Sun M, Dong Y, Zhang G, Qu J, Li J (2014) $\alpha$-Fe2O3 spherical nanocrystals supported on CNTs as efficient non-noble electrocatalysts for the oxygen reduction reaction. J Mater Chem A 2(33):13635–13640

[26] Sun M, Zhang G, Liu H, Liu Y, Li J (2015) $\alpha$- and $\gamma$-Fe2O3 nanoparticle/nitrogen doped carbon nanotube catalysts for high-performance oxygen reduction reaction. Sci China Mater 58(9):683–692

[27] Liu X, Hu W (2016) Iron oxide/oxyhydroxide decorated graphene oxides for oxygen reduction reaction catalysis: a comparison study. RSC Adv 6(35):29848–29854